Materials Science Forum
ISSN: 1662-9752, Vol. 1089, pp 63-69
doi:10.4028/p-666z18

Submitted: 2022-09-04
Revised: 2022-10-26
Accepted: 2022-11-25
Online: 2023-05-26

Selective Oxidation during AFM Electrical Characterization of Doped SiC Layers

R. Coq Germanicus[1,a*], A. Boumaarouf[1,b], C. Villeneuve-Faure[2,c], V. Shah[3,d], P. M. Gammon[3,e], U. Lüders[1,f]

[1]NORMANDIE UNIV, ENSICAEN, UNICAEN, CNRS, CRISMAT, 14000 Caen, France

[2]LAPLACE, Université de Toulouse, CNRS, INPT, UPS, 31077 Toulouse, France

[3]School of Engineering, University of Warwick, Coventry CV4 7AL, United Kingdom

[a]rosine.germanicus@unicaen.fr, [b]abdelhaq.boumaarouf@ensicaen.fr,
[c]christina.villeneuve@laplace.univ-tlse.fr, [d]vishal.shah@warwick.ac.uk,
[e]p.m.Gammon@warwick.ac.uk, [f]ulrike.luders@ensicaen.fr

Keywords: local oxidation, Atomic Force Microscopy, doped Silicon Carbide, MOSFET

Abstract. The possibility of anodic oxidation of SiC surfaces by a strong, local electric field applied during Atomic Force Microscopy (AFM) under ambient conditions is an interesting method to achieve nano-patterning of SiC, but is also a side-effect to be well characterized and controlled during this kind of AFM measurements if used to determine the local electric properties. In this contribution, we will analyze the local electric fields by finite element simulations in order to quantify the effect of the presence of a water meniscus and of an oxide layer on the SiC surface. Furthermore, we will experimentally highlight the strong influence of the local doping on the anodization, leading to the formation of thicker oxide layers at the location of highly doped SiC. Therefore, the location of these areas can be determined by a simple AFM topography scan after the application of a high field, allowing to detect highly doped SiC areas in complex structures as for example SiC MOSFETs.

Introduction

Since the emerging wide band semiconductor SiC MOSFET discrete devices showed their capabilities for electric power conversion with high frequency, high power and high temperature, for example power converter systems.

The high integration, process requirements and reliability of power devices require local analysis of the device at the SiC die level. Based on Atomic Force Microscopy (AFM), several modes are becoming essential techniques to probe local electrical properties. Scanning Capacitance Microscopy (SCM), Scanning Non-linear Dielectric Microscopy (SNDM), Conductive AFM (C-AFM) or Scanning Spreading Resistance Microscopy (SSRM) have demonstrated their capability in terms of spatial resolution, detection of active dopants or resistivity mapping. Mostly used in contact mode, during these AFM measurements a nano-contact is formed by the AFM conductive tip and the sample. This nano-contact is polarized with a DC and or an AC biases. When measurements are performed in ambient environment, the presence of water at the surface of the material can affect the electrical characterization, but even more, it may lead to a local oxidation of the sample due to the high electric field strength in the AFM tip area [1]. Concerning SiC, despite the relative chemical inertness and mechanical hardness of the semiconductor, previous studies reported that AFM Local Anodic Oxidation (AFM-LAO) is possible in air and at room temperature, during the scan. The underlying physical mechanism is based on the water molecule ionization by a local electrical field (larger than 10^7 V/m), leading to the dissolution and the transport of the oxyanions OH^- to form a local oxide on the SiC surface. Using this mechanism for nano-patterning (oxidized nano-structures like nano-dots or lines), some authors studied the AFM-LAO oxide growth rate for SiC as a function of the applied DC bias, loading force, scan rate and/or doping level of the SiC [2-6]. For example, by comparing experimental results for two doping levels of phosphorus-implanted 4H-SiC, the reference [6] showed that the AFM local oxidation can be promoted by high doping concentrations.

This contribution analyses the local anodic oxidation during AFM electrical measurements. The influence of the gradually increasing doping level of SiC layers is investigated. An as case study, results obtained for a commercial SiC MOSFET is presented.

Experimental Details

Two samples are studied. First, a wafer made of epitaxial SiC multilayers doped in situ with nitrogen (N) was characterized. The layers are deposited by Chemical Vapor Deposition (CVD) on a 4H-SiC substrate with a growth rate of 5 µm/h. The substrate is misoriented by 4° (angle between the surface normal and the c-axis) from the [11$\bar{2}$ 0] direction. The sample is then multilayered with dopant concentrations from 10^{16} to 10^{19} at/cm^3. Secondly, a commercial SiC MOSFET is studied. For the local measurements, cross section preparations were made. The wafer and discrete device were cutting perpendicularly to the surface and cross sections were polished with lapping films of decreasing granularity to obtain a mirror-like surface with very low roughness.

AFM measurements were performed using a Dimension Icon AFM from Bruker. Simultaneously, the topography and conductivity with C-AFM [7] mode were acquired using a metallized platinum-iridium (PtIr) coated tip (SCM-PIC, Bruker Corporation, USA). The AFM tip radius is 25 nm and the spring constant of the cantilever is 0.1 N/m. The pixel resolution was 512 × 512 pixels with a relatively slow scan rate about 0.3 Hz. Measurements are performed under ambient conditions: ambient temperature with a relative humidity of 45 %.

Results

Tip-SiC interaction during AFM measurements

In order to study AFM tip-SiC interactions, AFM force-displacement curves recorded in spectroscopy mode are studied. By acquiring the deflection of the AFM cantilever during the tip-sample interaction for the approach and retract steps, the applied force as a function of the displacement is determined. The force is calculated with the measured laser deflection, the spring constant determined by the thermal noise method and the sensitivity of the AFM cantilever. The adhesion signal is measured on the retracted curve (Fig. 1). This force is related to the water meniscus around the apex of the AFM tip. In fact, during the tip approach, the AFM cantilever is pulled down towards the surface to contact the SiC surface. Afterwards, the cantilever withdraws and the measured force decreases, until it reaches a minimum. This point determines the adhesion force, where the water meniscus opposes the movement of the cantilever. Without polarization, a significant force is measured, indicating the presence of the meniscus of water around the AFM tip (Fig. 1a). Moreover, an enhancement of the adhesion force is observed (Fig. 1b) with the application of a negative bias about -10 V. When a bias is applied, electrostatic forces are involved in the tip sample interaction. The force curves show that the adhesion force, between the AFM tip and the SiC surface, increases of a factor of 1.5 when a voltage of -10 V is applied to the tip.

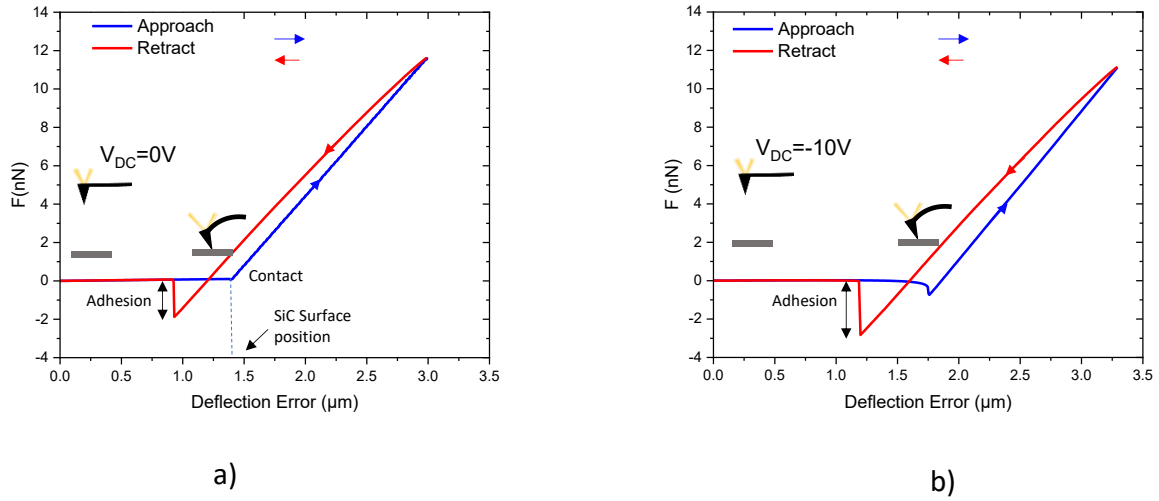

Fig. 1. AFM force curves for two applied DC bias a) V_{DC}= 0V and b) V_{DC}= -10 V. Approach and retract curves are represented, schematics of the cantilever position are added.

In C-AFM during the tip-sample interaction the current flowing from the tip through the back contact of the sample is recorded. The evolution of the current is reported in Fig. 2 for V_{DC} = -10 V. When the tip is in contact with the sample surface, the electric current is established, which is manifested by the drop. The C-AFM current between the conductive tip and the doped SiC reaches -2 pA. Experiment is recorded for the SiC layer with a doping level of 4 x 10^{17} at/cm^3.

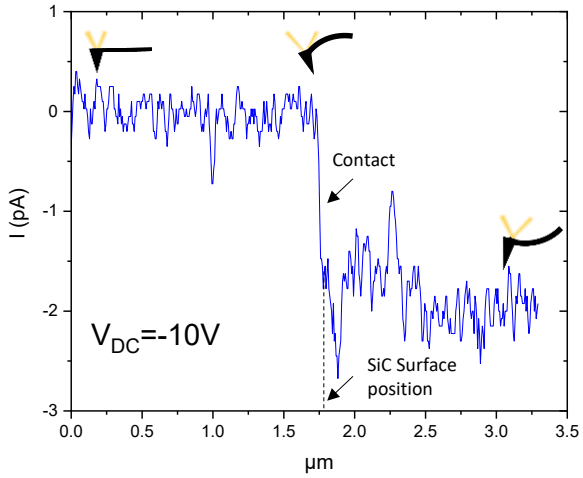

Fig. 2. Evolution of the collected C-AFM current during the approach step V_{DC}= -10 V

Electric field distribution

When a negative bias is applied between the AFM tip and the SiC, a localized electric field is generated. In air ambient, the electric field around the tip is the origin of the local oxidation. To compute this electric field in the water meniscus/oxide/SiC stack, an electrostatic modeling is required. A simple 2D-axisymmetric finite element model describing the AFM tip in a classical way is used: a truncated cone (10 µm height and 14° aperture angle) ending with a semi-spherical apex (curvature radius Rc = 25 nm). The tip is supposed to be surrounded by air, modeled by a box whose dimensions are large enough to avoid edge effects [8]. In our model the water meniscus is considered. The water meniscus is described by a height of 30 nm and a radius of 50 nm at the interface with the device. The device is modelled by a 500 nm-thick SiC layer covered by SiO_x layer whose thickness range from 0 nm to 6 nm. The relative dielectric permittivity of water, SiC and SiO_x is 80, 9.2 and 3.8, respectively.

For this, the Poisson's equation is solved in the surrounding air, the water meniscus and the device to determine the local electric fields $\vec{E}$.

$$div(\varepsilon\vec{E}) = \rho \quad (1)$$

where ρ is the charge density and ε the dielectric permittivity.
The electric field $\vec{E}$ derives from potential V in the following way:

$$\vec{E} = -\overrightarrow{grad}(V) \quad (2)$$

Typical boundary conditions were applied, no charge conditions (zero potential) on the free boundaries of the simulation box to avoid edge effects.
The water meniscus, SiOx and SiC are considered as free of charge (i.e. ρ=0 cm^{-3}).

With the finite element modelling, using Comsol Multiphysics software, the effect of the water meniscus is showed in Fig. 3. a and b. Without water, the electric field is strongly localized under the AFM tip (Fig. 3. a). The electric field is around 8.2 x 10^9 V/m at the contact point and it is divided by a factor 10 at 20 nm away from the contact point. In presence of the water meniscus, the electric field is more distributed over the contact area between the absorbed water and 4H-SiC (Fig. 3. c).

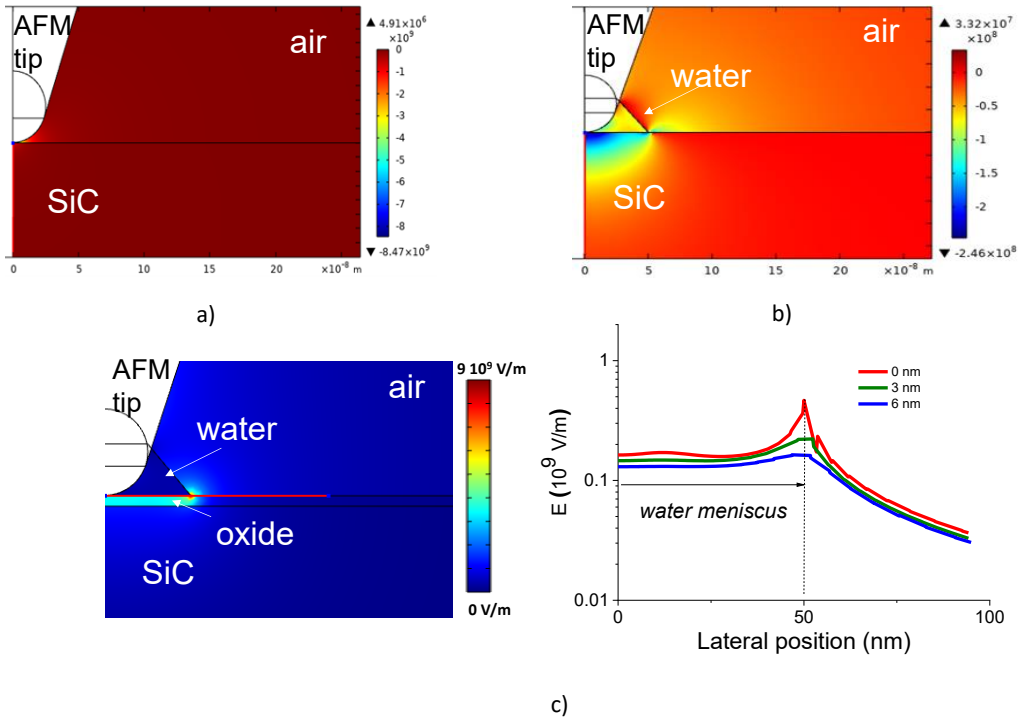

Fig. 3. Simulation of the electric field a) without water, b) with a water meniscus and c) with an oxide layer and calculated local electric field E profiles without oxide and with 2 nm and 6 nm.

With an oxide layer at the surface of the SiC, the electric field distributions are showed in Fig.3.c. An enhancement of the electric field inside the oxide layer and around the edge of the AFM tip is observed. Profiles of the electric field at the SiC surface, SiC/oxide interface and at the oxide surface are represented in Fig. 3.c), with the presence of the water meniscus. A high electric field is calculated at the surface of the oxide, just below the AFM tip. The electric field is quasi-constant over 40 nm with a value of 3.5 x 10^8 V/m. Moreover, a variation of the oxide thickness, between 2 nm and 6 nm, has a weak influence on the electric field. This result quantifies the effect of the oxide on the local electrical field distribution during AFM electrical measurements, but it also shows the length of the area subject to the strong field during the SiC local anodization.

Effect of the doping level

In order to evaluate the dependence of the doping effect, the multilayered sample was analyzed. Fig. 4 represents the AFM topography of n-doped 4H-SiC layers with different doping levels before and after the scan using a bias of – 10 V applied to the conductive tip. The scan size is 5 µm × 2.5 µm (with a resolution of 512 × 256 pixels). The evolution of the SIMS profile of the nitrogen doping is added on the AFM scans. After the sample preparation, the cross-sectional sample presents a low surface roughness R_q = 0.7 nm and R_a = 0.5 nm. By comparing the two topographies obtained at the same location, before (Fig.4 a) and after the C-AFM measurement (Fig.4 b) a modification of the surface is observed for the highly doped regions of the sample (zones 4 and 5, and the substrate in Fig. 4). This surface modification is related to the local oxidation of the SiC. The change in height of 2.8 nm, shown in the inset of Fig. 4 b, of the area with the highest doping concentration (zone 5) is accompanied by a roughness increase of the regions with slightly lower doping concentration (zones 4 and substrate). Here, it seems that the oxidation does not lead to a continuous film due to the local character of the tip-sample interaction, where the anodization occurs pixel by pixel during the AFM scan. To confirm the presence of an oxide layer (SiO_x or SiO_xC_y), currents collected by the tip-sample nano-contact were recorded simultaneously to the topography. Recorded current indicates a decrease of the local current after the modification of the surface (Figure 3 b)). The AFM-LO created a swelling of the surface by a preferred growth of an oxide layer on selective zones of the gradually doped sample.

Comparing the regions with a lower doping level (zones 1 to 3 and 6 in Fig. 4 a and b), no significant modification of the sample surface is observed. This is especially visible in zone 6, which becomes easily distinguishable in the topography measurement after the local anodization. The correlation between the doping level of the SiC sample and AFM-LAO intensity highlights the local surface oxidation, selectively on highly doped SiC areas, during C-AFM scanning when the tip is negatively biased.

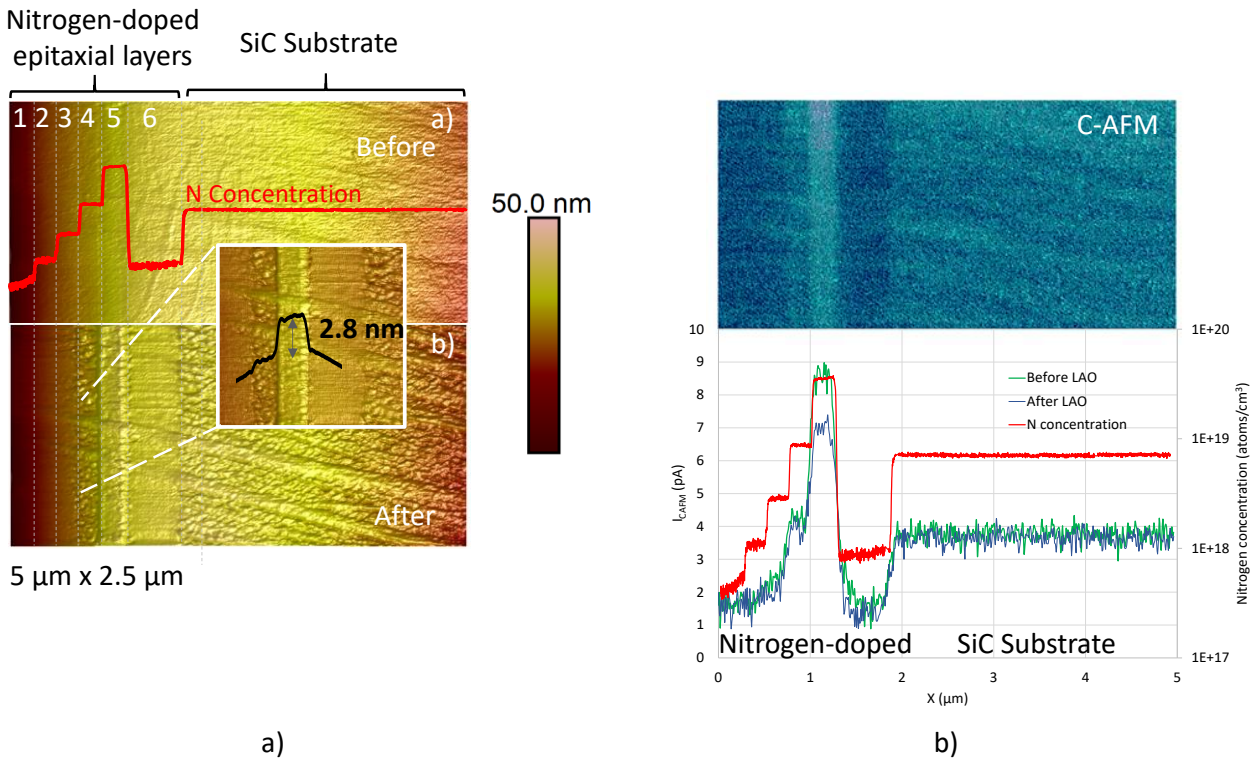

Fig. 4. a) AFM topographies before and after the AFM-LAO for the SiC doped staircase sample, the SIMS profile is reported and b) mapping of the current $I_{C\text{-}AFM}$ on the SiC surface by C-AFM measurements. The red curve shows the doping level of the sample as a function of the depth from SIMS measurements, the green and the blue curves the collected current after and before AFM-LAO.

Case study: AFM-LAO during a MOSFET measurement

The same experimental setup is applied to characterize a commercial SiC-MOSFET. Figure 5.a) reports the surface topographies before and after the application of the negative bias. Before local oxidation, the topography shows the MOS structure of the SiC device, the gate and the source contact. The topography in the area of the contact source is due to the different mechanical properties of the materials (SiC, oxide and metals). Inter-metal dielectric layers can be distinguished. For the second scan a negative bias of (-10 V) is applied. The topography shows supplementary areas with a topographic contrast, revealing a local oxidation of the SiC located on both sides of the MOS channel, at the location of the highly n-type doped layers. This surface modification can be noticed also for the n+ substrate region of the device. For the less doped regions (for example the n- drift layer), no oxide formation was detected for the used experimental parameters, as expected from the results of the previous section showing the strong dependence on the SiC doping level.

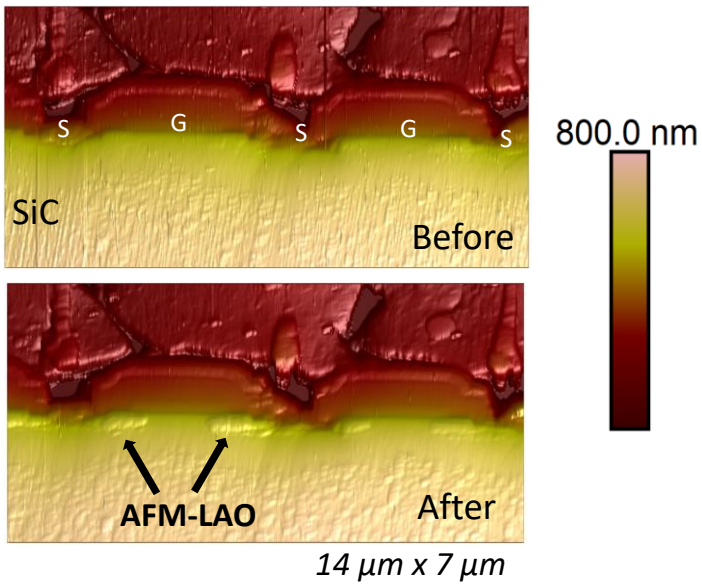

Fig. 5. a) AFM topographies before and after the AFM-local oxidation for a commercial SiC-MOSFET.

Conclusion

The signature of the water meniscus around the AFM tip is highlighted by the analysis of the AFM force-displacement curves in the spectroscopy mode. After the evaluation of the electric field by a comprehensive finite element modelling. Using a gradual doping SiC sample, doping level influence is evaluated, the oxide grows selectively on highly doped SiC areas, when the tip is negatively biased. In addition, results on a commercial SiC MOSFET device reveals the position of strongly doped areas in the complex structures, achieved by simple topography measurements after the application of a sufficient local electric field through the tip.

References

[1] Y.K. Ryu, A.W. Knoll, Springer, (2019).

[2] X.N. Xie, H.J. Chung, C.H. Sow, A.T.S. Wee, Applied Physics Letters: Vol 96 (2004).

[3] Y.D. Jo, S.H. Seo, W. Bahng, S.C Kim, N.K. Kim, S.S. Kim, S. M. Koo, Applied Physics Letters, 96(8), 082105. (2010).

[4] J.-J. Ahn, Y.-D. Jo, S.-C. Kim, J.-H. Lee, and S.-M. Koo, Nanoscale Research Letters, vol. 6 (2011).

[5] Lorenzoni, M., & Torre, B., Applied Physics Letters, 103(16), 163109 (2013).

[6] J. H. Lee, J. J. Ahn, A. Hallén, C.-M. Zetterling, and S. M. Koo, Materials Science Forum, (2012).

[7] P. Fiorenza, E. Schilirò, F. Giannazzo, C. Bongiorno, M. Zielinski, F. La Via, F. Roccaforte, Applied Surface Science, 526, 146656 (2020).

[8] F. Mortreuil, L. Boudou, K. Makasheva, G. Teyssedre and C. Villeneuve-Faure, Nanotechnology 32, 065706 (2021)